eJSE International

Electronic Journal of Structural Engineering 12(1) 2012

Seismic Response of Concrete Arch Dams Including Dam-Reservoir-Foundation Interaction Using Infinite Elements

H. Mirzabozorg
K. N. Toosi University of Technology, Iran, Mirzabozorg@kntu.ac.ir

A. Kordzadeh
K. N. Toosi University of Technology, Iran, kordzadeh@sina.kntu.ac.ir

M.A. Hariri-Ardebili
University of Colorado at Boulder, USA, mohammad.haririardebili@colorado.edu

ABSTRACT: In the present paper, a direct time domain procedure is used for dynamic linear and nonlinear analysis of the coupled system of reservoir-dam-foundation in 3D space. The foundation is assumed massed and infinite elements are used to model the semi-infinite medium via the far-end boundary of the foundation model. The nonlinear behavior of mass concrete is modeled using the smeared crack approach in which the elements can be cracked in each Gaussian point. The reservoir is assumed to be compressible and is modeled using finite element method with appropriate boundary conditions. The coupled system is solved using the staggered displacement method. As a case study, KARADJ double curvature arch dam in Iran is chosen to investigate the effect of massed foundation on the seismic response of the system. It is found that the response of the system with massed foundation including infinite elements is the same as that when the artificial absorbing boundary on the far-end boundary of the foundation is modeled using the viscous boundary. In addition, when the foundation is assumed mass-less, the resulted seismic stresses within the dam body can be too conservative. Decreasing the crack profiles and displacements are observed in nonlinear analysis of the dam when infinite elements are used to model the semi-infinite medium via the far-end boundary of the foundation model.

KEYWORDS: Arch dam, dam-reservoir-foundation interaction, infinite element, smeared crack model

1 INTRODUCTION

Considering an arch dam to be adequately massive and stiff, while the foundation is relatively soft, the motion at the base of the structure may be significantly different from the free-field surface motion. However, it is apparent that the most of interaction effects occurs near the structure and at some finite distance from the base of the structure. Therefore, the field behavior converges back to the free field state.

During the past decades, various methods have been developed to analyze concrete gravity and arch dams with different assumptions and complexities concerning on the interaction effects of reservoir and foundation of the system. There are several investigations in the frequency domain in which the effect of the foundation is taken into account. The computer program, EAGD-84 is one of the most well-known software that is based on the finite element method and has the capability to analyze the coupled system of concrete gravity dams in 2D space including the foundation interaction effect (Fenves and Chopra, 1984). The effect of foundation interaction in this program is accounted using the impedance matrix of the foundation medium. EACD-3D (Fok et al., 1986) is the well-known code in analyzing concrete dams in 3D space. Tan and Chopra used the boundary element method to compute the impedance matrix and they analyzed the dam-reservoir foundation in the frequency domain (Tan and Chopra, 1995).

The above procedures are applicable in frequency domain analyses, which are used for linear problems. Therefore, an appropriate procedure in time domain must be represented to account for the interaction effect of the foundation on the seismic response of dam-reservoir-foundation system. For the dam problem, the influence of the reservoir on the dam response is also very important. Some outstanding work on reservoir-dam-foundation problem interaction in the frequency domain or the indirect time domain has been carried out by Chopra and his coworkers which some of them were pointed out. The reservoir-dam-foundation interaction problem has been studied in the time domain by Antes and Estorff (1987) using the full space transient Green's functions for wave propagation in both the founda-

tion and the reservoir. In the work presented by Gaun et al. (1994), an efficient numerical procedure has been described to investigate the dynamic response of a reservoir-dam-foundation system directly in the time domain. The dam has been modeled by the finite element method and the dynamic soil-structure interaction has been included by computing the impedance of the half-space. The reservoir influence on the dam was applied using the added mass approach. Mirzabozorg et al. (2003) presented a paper in which the linear behavior of the dam-reservoir system is modeled using finite element method in 3D space. Ghaemian et al. (2006) studied the effects of the foundation shape and mass on the linear seismic response of arch dams using finite element method including structure-reservoir interaction.

For modeling the nonlinear behavior of the mass concrete, various numerical models have been developed during recent years. In this regard, theories based on plasticity and fracture mechanics approaches are developed and used in most of engineering analyses. Kuo (1982) suggested interface smeared crack approach to model the contraction joints for dynamic analysis of arch dams. Dungar (1987) used a bounding surface model for static analysis of an arch dam. Cervera et al. (1995) utilized a continuum damage model to analyze Talvacchia arch dam in Italy. Noruziaan (1995) applied bounding surface and orthogonal smeared crack models for compressive and tensile regions of stresses, respectively in arch dams. Hall (1998) proposed a simple smeared crack model for modeling the contraction and construction joints in dynamic analysis of arch dams. Espandar and Lotfi (2002) employed non-orthogonal smeared crack approach and elasto-plastic models on the nonlinear analysis of Shaheed-Rajaee arch dam in Iran. In 2004, Mirzabozorg et al. utilized the damage mechanics approach to conduct the seismic nonlinear analysis of concrete gravity dams in 2D space including the dam-reservoir interaction effects. In the same line of thought, Mirzabozorg and Ghaemian (2005) developed a model based on the smeared crack approach in 3D space. Ardakanian et al. (2006) considered the nonlinear seismic behavior of mass concrete in 3D space which is based on an anisotropic damage mechanics model. Finally, an approach based on the fracture mechanics is developed so that the cracking within an element is non-uniform and candidate elements crack in Gaussian points (2007).

In the present paper, appropriate 3D infinite elements are utilized to model the radiation damping on the far-end boundary of the foundation medium. The smeared crack approach presented in (Mirzabozorg et al., 2007) is utilized to model the nonlinear behavior of the mass concrete. The staggered displacement method is used to solve the coupled problem of the dam-reservoir-foundation system and the developed numerical algorithm is utilized to simulate the nonlinear behavior of arch dams including the massed foundation, semi infinite medium at the far end boundary of the foundation and the compressible reservoir upstream of the dam body.

2 FOUNDATION INTERACTION AND WAVE PROPAGATION

One of the main aspects in the seismic loading and wave propagation within the semi-infinite medium such as rock underlying structures is preventing the wave reflection from the artificial boundary of the infinite medium in the finite element analysis. One of the most promising procedures in 3D problems is infinite elements. Using the infinite elements, the stiffness and the damping pertinent to the semi-infinite medium via the artificial boundary of the structure are accounted for in the analyses. The basic idea in utilizing infinite elements is to use the elements with the special shape functions for the geometry at the far-end truncated boundary. Therefore, there will be two sets of shape functions, the standard shape function, N_i, and a growth shape function, M_i. The growth shape function, M_i, grows without limit as the coordinate of i^{th} node approaches infinity, and is applied to the geometry. The standard shape functions N_i are applied to the field variables (Ross, 2004). A classic example is the line element which is depicted in Figure 1.

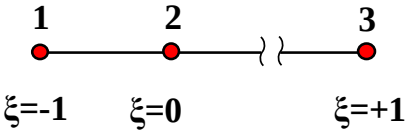

Figure 1. Line Element with Node 3 at Infinite

The geometric properties within the element are interpolated as:

$$x = M_1 x_1 + M_2 x_2 \tag{1}$$

$$M_1 = -\frac{2\xi}{1-\xi} \quad , \quad M_2 = \frac{1+\xi}{1-\xi} \tag{2}$$

where, x_i is the coordinate of the i^{th} node in global coordinate system and ξ is the coordinate in local system. The formation of the property matrices (i.e. the stiffness matrix) proceeds in the standard method, except the mapping function M_1 and M_2 are used to form the Jacobian matrix, [J]. According to Bettes in 1992, the growth shape functions, Mi, and their derivatives are presented in Table 1 for a 20-node solid element with a face in the infinity (Figure 2).

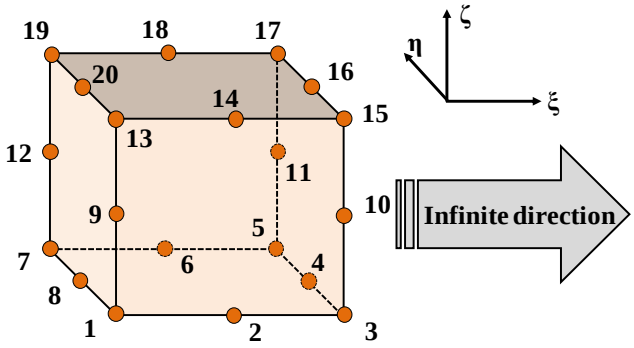

Figure 2. Solid Element with One Face in Infinity

The procedure for the formation of the stiffness matrix is as follows:

- Form the Jacobian matrix, [*J*], with the relative growth shape functions and their derivatives as given in Equation (1),

$$[J]=\begin{bmatrix}\frac{\partial M}{\partial \xi}\\ \frac{\partial M}{\partial \eta}\\ \frac{\partial M}{\partial \zeta}\end{bmatrix}[X\ Y\ Z] \tag{3}$$

where *X*, *Y* and *Z* are nodal coordinate vectors of the element.

- Invert [*J*] to achieve $[J]^{-1}$.
- Use the parent finite element shape functions, N_i, to obtain the matrix [*B*],

$$[B]=[J]^{-1}\begin{bmatrix}\frac{\partial N}{\partial \xi}\\ \frac{\partial N}{\partial \eta}\\ \frac{\partial N}{\partial \zeta}\end{bmatrix} \tag{4}$$

where [*B*] is the matrix transforming the nodal displacement of the considered element to the Gaussian point strains within the element.

- Form the stiffness matrix of the element, [K]

Finally, the effect of semi-infinite medium via the far-end boundary of the foundation is taken into account when obtained stiffness matrices and their related proportional damping matrices are assembled into the global stiffness matrix and the global damping matrix of the system.

3 CONSTITUTIVE LAW FOR MASS CONCRETE

The numerical model used for the nonlinear seismic analysis of the mass concrete in the present study can be found in (Mirzabozorg et al., 2007) in detail. The utilized approach is able to simulate the behavior of the mass concrete during the following phases:

- Pre-softening behavior
- Fracture energy conservation
- Non-linear behavior during the softening phase
- Crack closing/reopening behavior.

In the utilized numerical model, the uni-axial strain energy is used as the softening initiation criterion. In addition, the effect of loading rates on the apparent stress-strain curve is applied by a dynamic magnification factor, DMF_e, which is used on the strain energy as reported in (Mirzabozorg et al., 2007).

During the softening phase, the elastic stress-strain relationship is substituted with an anisotropic modulus matrix, which corresponds to the stiffness degradation level in the three principal directions. In this study, the secant modulus stiffness approach (SMS) is unitized for the stiffness formulation in which the constitutive relation is defined in terms of total stresses and strains as presented in Figure 3.

Table 1. Growth Shape Functions and Their Derivatives for One Face in Infinity

node *i*	M_i	$\partial M_i/\partial\xi$	$\partial M_i/\partial\eta$	$\partial M_i/\partial\zeta$
1	-(1-η)(1-ζ)(2+ξ+η+ζ)/2(1-ξ)	-(1-η)(1-ζ)(3+η+ζ)/2(1-ξ)^2	(1-ζ)(1+ξ+2η+ζ)/2(1-ξ)	(1-η)(1+ξ+η+2ζ)/2(1-ξ)
2	(1+ξ)(1-η)(1-ζ)/4(1-ξ)	(1-η)(1-ζ)/4(1-ξ)^2	-(1+ξ)(1-ζ)/4(1-ξ)	-(1+ξ)(1-η)/4(1-ξ)
6	(1+ξ)(1+η)(1-ζ)/4(1-ξ)	(1+η)(1-ζ)/4(1-ξ)^2	(1+ξ)(1-ζ)/4(1-ξ)	-(1+ξ)(1+η)/4(1-ξ)
7	-(1+η)(1-ζ)(2+ξ-η+ζ)/2(1-ξ)	-(1+η)(1-ζ)(3-η+ζ)/2(1-ξ)^2	-(1-ζ)(1+ξ-2η+ζ)/2(1-ξ)	(1+η)(1+ξ-η+2ζ)/2(1-ξ)
8	(1-η)(1+η)(1-ζ)/(1-ξ)	(1-η)(1+η)(1-ζ)/(1-ξ)^2	-2η(1-ζ)/(1-ξ)	-(1-η)(1+η)/(1-ξ)
9	(1-η)(1-ζ)(1+ζ)/(1-ξ)	(1-η)(1-ζ)(1+ζ)/(1-ξ)^2	-(1-ζ)(1+ζ)/(1-ξ)	-2ζ(1-η)/(1-ξ)
12	(1+η)(1-ζ)(1+ζ)/(1-ξ)	(1+η)(1-ζ)(1+ζ)/(1-ξ)^2	(1-ζ)(1+ζ)/(1-ξ)	-2ζ(1+η)/(1-ξ)
13	(1-η)(1+ζ)(-2-ξ-η+ζ)/2(1-ξ)	(1-η)(1+ζ)(-3-η+ζ)/2(1-ξ)^2	-(1+ζ)(-1-ξ-2η+ζ)/2(1-ξ)	(1-η)(-1-ξ-η+2ζ)/2(1-ξ)
14	(1+ξ)(1-η)(1+ζ)/4(1-ξ)	(1-η)(1+ζ)/4(1-ξ)^2	-(1+ξ)(1+ζ)/4(1-ξ)	(1+ξ)(1-η)/4(1-ξ)
18	(1+ξ)(1+η)(1+ζ)/4(1-ξ)	(1+η)(1+ζ)/4(1-ξ)^2	(1+ξ)(1+ζ)/4(1-ξ)	(1+ξ)(1+η)/4(1-ξ)
19	(1+η)(1+ζ)(-2-ξ+η+ζ)/2(1-ξ)	(1+η)(1+ζ)(-3+η+ζ)/2(1-ξ)^2	(1+ζ)(-1-ξ+2η+ζ)/2(1-ξ)	(1+η)(-1-ξ+η+2ζ)/2(1-ξ)
20	(1-η)(1+η)(1+ζ)/(1-ξ)	(1-η)(1+η)(1+ζ)/(1-ξ)^2	-2η(1+ζ)/(1-ξ)	(1-η)(1+η)/(1-ξ)

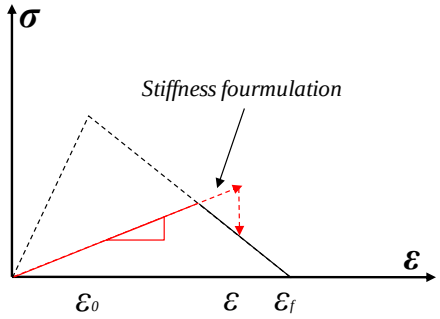

Figure 3. SMS Formulation of the Stiffness Modulus Matrix

The stiffness modulus matrix obtained using the smeared crack propagation model is given in Equation 5:

$$\left[D_G\right]_{nst}=\begin{bmatrix} D_{11} & D_{12} & D_{13} & 0 & 0 & 0 \\ D_{12} & D_{22} & D_{23} & 0 & 0 & 0 \\ D_{13} & D_{23} & D_{33} & 0 & 0 & 0 \\ 0 & 0 & 0 & D_{44} & 0 & 0 \\ 0 & 0 & 0 & 0 & D_{55} & 0 \\ 0 & 0 & 0 & 0 & 0 & D_{66} \end{bmatrix} \tag{5}$$

where;

$$D_{11}=\frac{\eta_1 E\left(1-\upsilon^2\eta_2\eta_3\right)}{1-\upsilon^2\eta_1\eta_2-\upsilon^2\eta_2\eta_3-\upsilon^2\eta_1\eta_3-2\upsilon^3\eta_1\eta_2\eta_3}$$

$$D_{22}=\frac{\eta_2 E\left(1-\upsilon^2\eta_1\eta_3\right)}{1-\upsilon^2\eta_1\eta_2-\upsilon^2\eta_2\eta_3-\upsilon^2\eta_1\eta_3-2\upsilon^3\eta_1\eta_2\eta_3}$$

$$D_{33}=\frac{\eta_3 E\left(1-\upsilon^2\eta_1\eta_2\right)}{1-\upsilon^2\eta_1\eta_2-\upsilon^2\eta_2\eta_3-\upsilon^2\eta_1\eta_3-2\upsilon^3\eta_1\eta_2\eta_3}$$

$$D_{12}=\frac{\upsilon\eta_1\eta_2 E\left(1+\upsilon\eta_3\right)}{1-\upsilon^2\eta_1\eta_2-\upsilon^2\eta_2\eta_3-\upsilon^2\eta_1\eta_3-2\upsilon^3\eta_1\eta_2\eta_3}$$

$$D_{23}=\frac{\upsilon\eta_2\eta_3 E\left(1+\upsilon\eta_1\right)}{1-\upsilon^2\eta_1\eta_2-\upsilon^2\eta_2\eta_3-\upsilon^2\eta_1\eta_3-2\upsilon^3\eta_1\eta_2\eta_3}$$

$$D_{13}=\frac{\upsilon\eta_1\eta_3 E\left(1+\upsilon\eta_2\right)}{1-\upsilon^2\eta_1\eta_2-\upsilon^2\eta_2\eta_3-\upsilon^2\eta_1\eta_3-2\upsilon^3\eta_1\eta_2\eta_3} \tag{6}$$

$$D_{44}=\beta_{12}G$$

$$D_{55}=\beta_{23}G$$

$$D_{66}=\beta_{13}G$$

in which, E, υ, η_1, η_2 and η_3 are initial Young's modulus in isotropic mass concrete, Poisson's ration of mass concrete, the ratios of the softened Young's modulus in the three principal directions to the initial isotropic elastic modulus and β_{12}, β_{23} and β_{13} are the shear stiffness factors corresponding to the principal directions given as:

$$\beta_{12}=\frac{(1+\upsilon)\left(\frac{\eta_1\varepsilon_1-\eta_2\varepsilon_2}{\varepsilon_1-\varepsilon_2}+\frac{\upsilon\eta_3\left(\eta_1-\eta_2\right)\varepsilon_3}{\varepsilon_1-\varepsilon_2}-\upsilon\eta_1\eta_2-2\upsilon^2\eta_1\eta_2\eta_3\right)}{1-\upsilon^2\eta_1\eta_2-\upsilon^2\eta_2\eta_3-\upsilon^2\eta_1\eta_3-2\upsilon^3\eta_1\eta_2\eta_3}$$

$$\beta_{23}=\frac{(1+\upsilon)\left(\frac{\eta_2\varepsilon_2-\eta_3\varepsilon_3}{\varepsilon_2-\varepsilon_3}+\frac{\upsilon\eta_1\left(\eta_2-\eta_3\right)\varepsilon_1}{\varepsilon_2-\varepsilon_3}-\upsilon\eta_2\eta_3-2\upsilon^2\eta_1\eta_2\eta_3\right)}{1-\upsilon^2\eta_1\eta_2-\upsilon^2\eta_2\eta_3-\upsilon^2\eta_1\eta_3-2\upsilon^3\eta_1\eta_2\eta_3}$$

$$\beta_{13}=\frac{(1+\upsilon)\left(\frac{\eta_1\varepsilon_1-\eta_3\varepsilon_3}{\varepsilon_1-\varepsilon_3}+\frac{\upsilon\eta_2\left(\eta_1-\eta_3\right)\varepsilon_2}{\varepsilon_1-\varepsilon_3}-\upsilon\eta_1\eta_3-2\upsilon^2\eta_1\eta_2\eta_3\right)}{1-\upsilon^2\eta_1\eta_2-\upsilon^2\eta_2\eta_3-\upsilon^2\eta_1\eta_3-2\upsilon^3\eta_1\eta_2\eta_3} \tag{7}$$

The constitutive matrix in Equation 5 is transformed to the global co-ordinate system as following:

$$\left[D_G\right]_G=\left[T\right]^T\left[D_G\right]_{nst}\left[T\right] \tag{8}$$

where [T] is the strain transformation matrix in 3D space. Based on the maximum strain reached in each principal direction, the secant modulus matrix is determined. Increasing the normal strain in each principal direction leads to the reduction of the corresponding softened Young's modulus. Finally, when the maximum strain reaches the fracture strain, the considered Gaussian point within the element is fully cracked and its contribution in the stiffness matrix of the element is eliminated in the corresponding direction. It is worth noting that the proposed model falls into Co-axial Rotating Crack Model (CRCM) category in which the local axes of the obtained modulus matrix, Equation 5, is always kept aligned with the directions of principal strains in the considered Gaussian point.

4 FLUID- STRUCTURE INERACTION AND THE COUPLED PROBLEM

The governing equation in the reservoir medium is Helmoltz equation from the Euler's equation given as (Mirzabozorg et al., 2003):

$$\nabla^2 p=\frac{1}{C^2}\frac{\partial^2 p}{\partial t^2} \tag{9}$$

where p, C and t are the hydrodynamic pressure, pressure wave velocity in the liquid and time, respectively. Boundary conditions required to apply on the reservoir medium to solve Equation 9 are explained in (Bettess, 1992). These boundaries are schematically demonstrated in Figure 4.

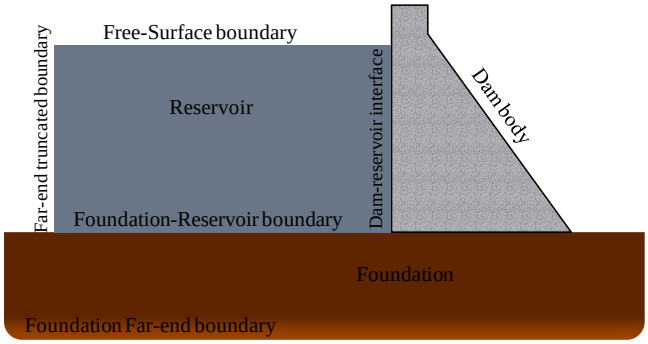

Figure 4. Reservoir boundary conditions

The equations of the dam-foundation (as the structure) and the reservoir take the form:

$$\begin{cases} [M]\{\ddot{U}\}+[C]\{\dot{U}\}+[K]\{U\} \\ \quad =\{f_1\}-[M]\{\ddot{U}_g\}+[Q]\{P\}=\{F_1\}+[Q]\{P\} \\ [G]\{\ddot{P}\}+[C']\{\dot{P}\}+[K']\{P\} \\ \quad =\{F\}-\rho[Q]^T\left(\{\ddot{U}\}+\{\ddot{U}_g\}\right)=\{F_2\}-\rho[Q]^T\{\ddot{U}\} \end{cases} \quad (10)$$

where [*M*], [*C*] and [*K*] are the mass, damping and stiffness matrices of the structure including the dam body and its foundation media and [*G*], [*C'*] and [*K'*] are matrices representing the mass, damping and stiffness equivalent matrices of the reservoir, respectively. The matrix [*Q*] is the coupling matrix; {f_1} is the vector including both the body and the hydrostatic force; {*P*} and {*U*} are the vectors of hydrodynamic pressures and displacements, respectively and {$\ddot{U}_g$} is the ground acceleration vector. A detailed definition of matrices and vectors used in Equation 10 has been provided in (Mirzabozorg et al., 2003). The coupled equations (12) are solved using the staggered displacement method in which the direct integration scheme is used to determine the displacement and hydrodynamic pressure at time increment *i+1*. The α-method is utilized for discretization of both equations (implicit–implicit method). In this method, the velocity and displacement at time step *i+1* can be written as:

$$\{\dot{U}\}_{i+1}=\{\dot{U}\}_{i+1}^{P}+\gamma\Delta t\{\ddot{U}\}_{i+1} \quad (11)$$
$$\{\dot{U}\}_{i+1}^{P}=\{\dot{U}\}_{i}+(1-\gamma)\Delta t\{\ddot{U}\}_{i}$$
$$\{U\}_{i+1}=\{U\}_{i+1}^{P}+\beta\Delta t^2\{\ddot{U}\}_{i+1} \quad (12)$$
$$\{U\}_{i+1}^{P}=\{U\}_{i}+\Delta t\{\dot{U}\}_{i}+(0.5-\beta)\Delta t^2\{\ddot{U}\}_{i}$$

where, γ and β are the integration parameters. The similar equations can be written for determining $\{\dot{P}\}_{i+1}^{P}$, $\{P\}_{i+1}$ and $\{P\}_{i+1}^{P}$. The terms with superscript *p* represent displacement, velocity and pressure quantities at time step *i+1* which are obtained using the pertinent quantities at time step *i*.

The governing field equations at time *i+1* can be written as:

$$[M]\{\ddot{U}\}_{i+1}+[C]\{\dot{U}\}_{i+1}+(1+\alpha)[K]\{U\}_{i+1} =\{F_1\}_{i+1}+[Q]\{P\}_{i+1}+\alpha[K]\{U\}_{i} \quad (13)$$

$$[G]\{\ddot{P}\}_{i+1}+[C']\{\dot{P}\}_{i+1}+(1+\alpha)[K']\{P\}_{i+1} =\{F_2\}_{i+1}-\rho[Q]^T\{\ddot{U}\}_{i+1}+\alpha[K']\{P\}_{i} \quad (14)$$

where, α is related to the numerical damping of the solver algorithm. The coupled field equations 13 and 14 are solved using the staggered displacement solution scheme (Mirzabozorg et al., 2003). In this method, equation 13 is approximated as:

$$[M]\{\ddot{U}\}_{i+1}^{*}=\{F_1\}_{i+1}+[Q]\{P\}_{i+1}^{p}-[C]\{\dot{U}\}_{i+1}^{p} -(1+\alpha)[K]\{U\}_{i+1}^{p}+\alpha[K]\{U\}_{i} \quad (15)$$

Combining equations 13 and 15 using equations 11 and 12 gives:

$$[M]\{\ddot{U}\}_{i+1}=[M]\{\ddot{U}\}_{i+1}^{*}+\beta\Delta t^2[Q]\{\ddot{P}\}_{i+1} -\gamma\Delta t[C]\{\ddot{U}\}_{i+1}-(1+\alpha)\beta\Delta t^2[K]\{\ddot{U}\}_{i+1} \quad (16)$$

The lumped mass results in a diagonal mass matrix. This property is utilized in modifying equation 16 such that:

$$[M]\{\ddot{U}\}_{i+1}=[M]\{\ddot{U}\}_{i+1}^{*}+\beta\Delta t^2[Q]\{\ddot{P}\}_{i+1} \quad (17)$$

Substituting equation 17 into equation 14 then:

$$\left([G]+\rho\beta\Delta t^2[Q]^T[M]^{-1}[Q]\right)\{\ddot{P}\}_{i+1} +[C']\{\dot{P}\}_{i+1}+(1+\alpha)[K']\{P\}_{i+1} =\{F_2\}_{i+1}-\rho[Q]^T\{\ddot{U}\}_{i+1}^{*}+\alpha[K']\{P\}_{i} \quad (18)$$

In equation 18, the right hand side terms are known; thus, $\{P\}_{i+1}$ is obtained. In order to correct the approximation made in equation 17, $\{P\}_{i+1}$ is substituted in equation 13 to calculate $\{U\}_{i+1}$ and its derivatives. The procedure of the staggered displacement method is summarized by the following steps:

- Step 1: Knowing the displacement, velocity and pressure at time i, $\{\ddot{U}\}_{i+1}^{*}$ is obtained from equation 15.
- Step 2: $\{\ddot{U}\}_{i+1}^{*}$ is introduced in equation 18 to calculate $\{P\}_{i+1}$

- Step 3: $\{P\}_{i+1}$ is substituted into equation 13 to calculate $\{U\}_{i+1}$ and its derivatives.

5 FINITE ELEMENT IMPLEMENTATION AND NUMERICAL SOLUTION

The 20-node iso-parametric "brick" finite elements are implemented to model the structure, mathematically. The requirement for integration and generation of the mass, stiffness and damping matrices for this type of element is 27 Gaussian points in 3*3*3 order within each element. Figure 5 shows the ordering of the Gaussian points within the elements. It is worthy to note that in the smeared crack approach, cracking process is applied on each Gaussian point within the elements (Mirzabozorg et al., 2007).

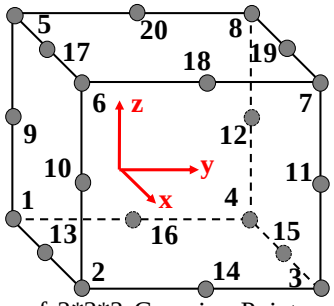

Figure 5. Ordering of 3*3*3 Gaussian Points within 20-Node Solid Elements

Based on the implemented algorithm, strains are computed and the cracking initiation criterion is checked in each Gaussian points. Cracking in each Gaussian point is simply modeled by adjusting the modulus stiffness matrix contribution of the considered point in the element stiffness matrix which is co-axial with the principal strain directions.

The foundation in the near field is modeled using 20-node solid elements and the infinite elements with one face at the infinity are used to simulate the semi-infinite medium via the far-end boundary of the foundation model. Finally, the fluid domain is modeled using 8-node fluid elements in which the DOF at their nodes is the hydrodynamic pressure.

KARADJ dam, located in Iran, is selected to obtain the effects of the foundation interaction on the seismic response of the structure. The dam is double curvature arch dam with the height of 168m and its crest length is 390m. The dam structure is modeled with 72 iso-parametric 20-node elements and its foundation medium surrounding the dam body is simulated using 980 elements in which the number of the infinite elements at the far-end boundary of the foundation is 240. Note that the depth of the foundation FE is about twice of the dam height in the three global directions.

The fluid is modeled using 1024 iso-parametric 8-node fluid elements and is extended about twice of the height of the dam body in the upstream direction. Figure 6 illustrate the finite element model of the dam body, foundation and the reservoir, respectively.

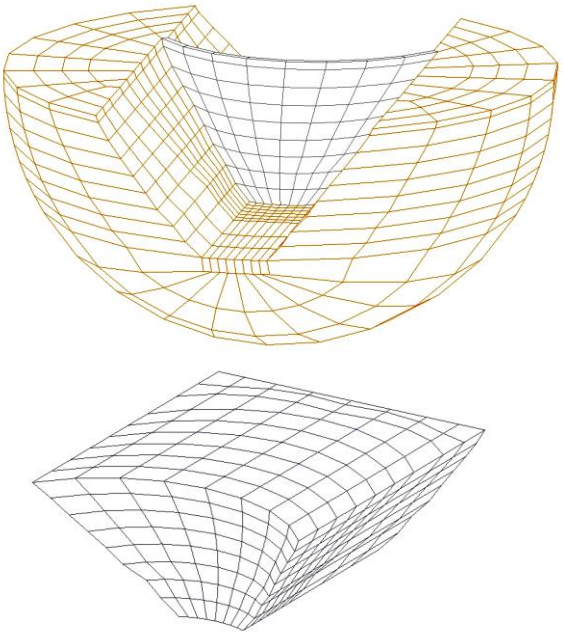

Figure 6. Finite element model of the dam body, the surrounding foundation and the reservoir

The modulus of elasticity, Poisson's ratio, the unit weight, the true tensile strength and the ratio of the apparent to the true tensile strength, the specific fracture energy and the dynamic magnification factor applied on both the tensile strength and the specific fracture energy are 26GPa, 0.17, 24.027kN/m^3, 3.662MPa, 1.35, 150N/m and 1.20, respectively. For the foundation medium, the modulus of elasticity, Poisson's ratio and the unit weight are taken as 16.3GPa, 0.15 and 29.400kN/m^3. The velocity of wave propagation and the unit weight of water in the reservoir are assumed 1436m/s and 9.807kN/m^3, respectively. The wave reflection coefficient of the reservoir bottom and sides is given as 0.8, conservatively.

The stiffness proportional damping is used in the conducted analyses in which the damping ratio for the fundamental mode is considered 10%. Applied loads on the system are the self weight, the hydrostatic pressure and the seismic load. The values of the integration parameters in the α-method are taken as α=-0.2, β=0.36 and γ=0.7. The quasi-linear damping mechanism is used for the structure in the dynamic analysis in which the stiffness proportional damping is updated during the element cracking within the dam body.

Figure 7 shows three components of the ground motion recorded at the Ab-bar station during Manjil earthquake on 20 June 1990 which is chosen for the analyses. This record is normalized and filtered for

the KARADJ dam site. The horizontal and vertical PGA's at maximum credible level (MCL) are 0.43g and 0.33g at the dam site, respectively. It is required to mention that all the components are multiplied by 1.5 to cause crack profiles within the dam body.

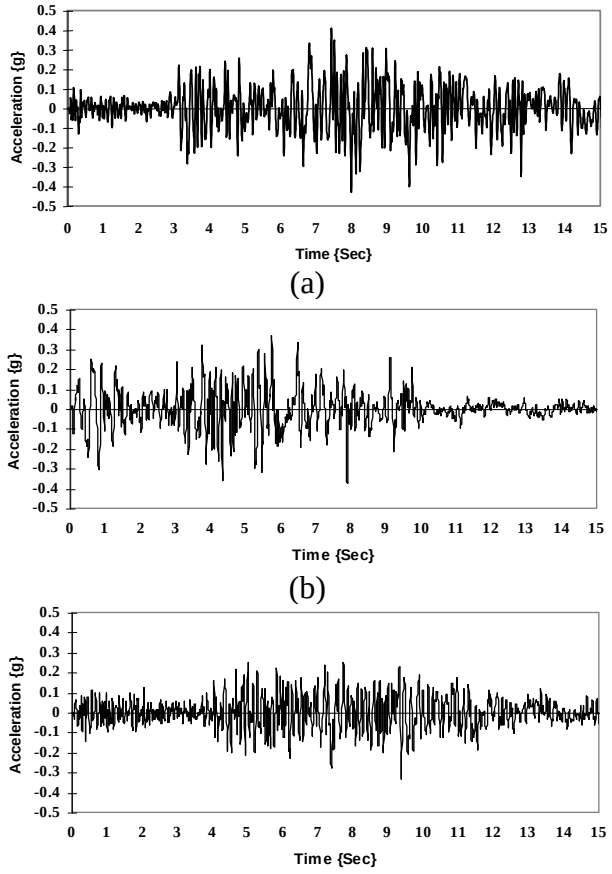

Figure 7. Components of the Manjil Earthquake on June 20, 1990, (a) US/DS component; (b) Cross-stream component; (c) Vertical component

6 RESULTS OF LINEAR MODEL

The three conducted analyses are; FE model of dam-reservoir-foundation assuming mass-less foundation; FE model of dam-reservoir-foundation assuming massed foundation and viscous boundary on the far-end truncated boundary of the foundation; and finally, FE model of dam-reservoir-foundation assuming massed foundation and implementing infinite elements for modeling the semi-infinite medium via the far-end truncated boundary of the foundation.

Figure 8 shows the crest response of the dam body in upstream/downstream (US/DS), cross-stream and vertical direction. It can be observed that considering infinite elements and viscous boundary (Ghaemian et al., 2006) on the far-end boundary of the foundation region decrease the crest response of the system in comparison with the system with mass-less foundation. However, there is not any noticeable difference between the results obtained from various conditions of the foundation in the cross stream direction.

Figures 9 and 10 illustrate contours of the cantilever and arch stresses in upstream and downstream faces of the dam body. As shown, the stresses obtained from the linear model with the massed foundation are less than the arch and cantilever stresses when the foundation is assumed mass-less. It is worthy to note that, when the far-end boundary of the massed foundation is modeled using viscous boundary (Ghaemian et al., 2006) or infinite elements, the obtained stress distribution within the dam body are the same.

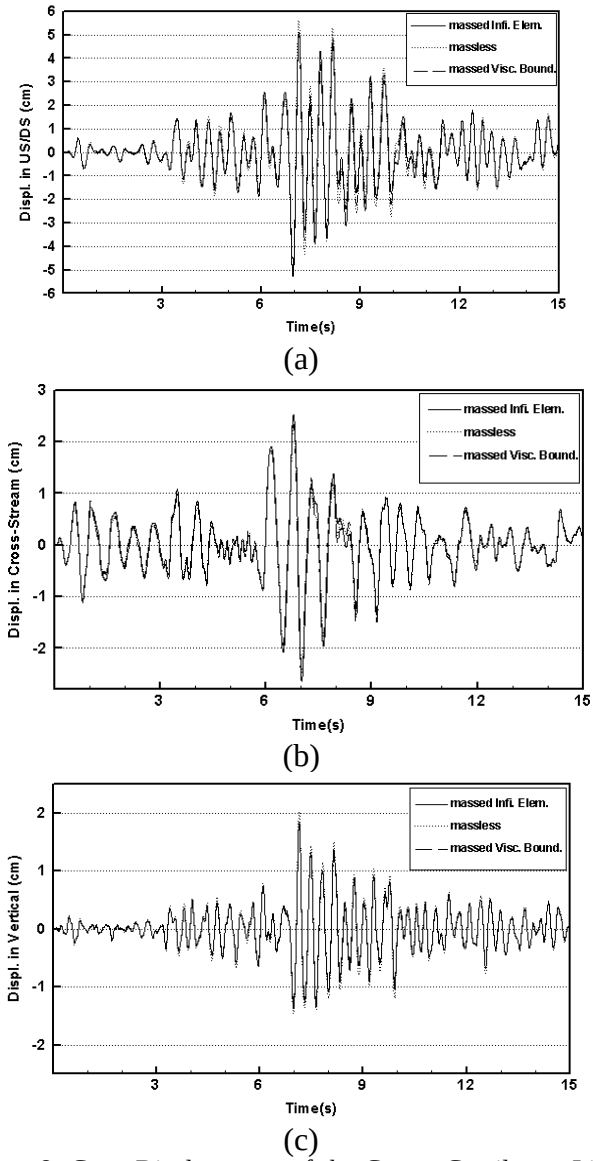

Figure 8: Crest Displacement of the Crown Cantilever; Linear analyses, (a) US/DS component; (b) Cross-stream component; (c) Vertical component

Table 2 presents the summary of the maximum tensile stresses resulted from the seismic analyses. The effect of massed foundation on cantilever stresses is much more than those on the arch stresses. The results obtained from the two models of massed foundation are approximately the same.

When the semi infinite medium via the far-end boundary of the foundation is modeled using infinite elements, the maximum arch and cantilever stresses are reduced 5.2% and 47.5%, respectively, in comparison with the model using mass-less foundation. These reductions reach to 7.4% and 44.1%, respectively, when the far-end boundary of the foundation is constrained for the case of the viscous boundary.

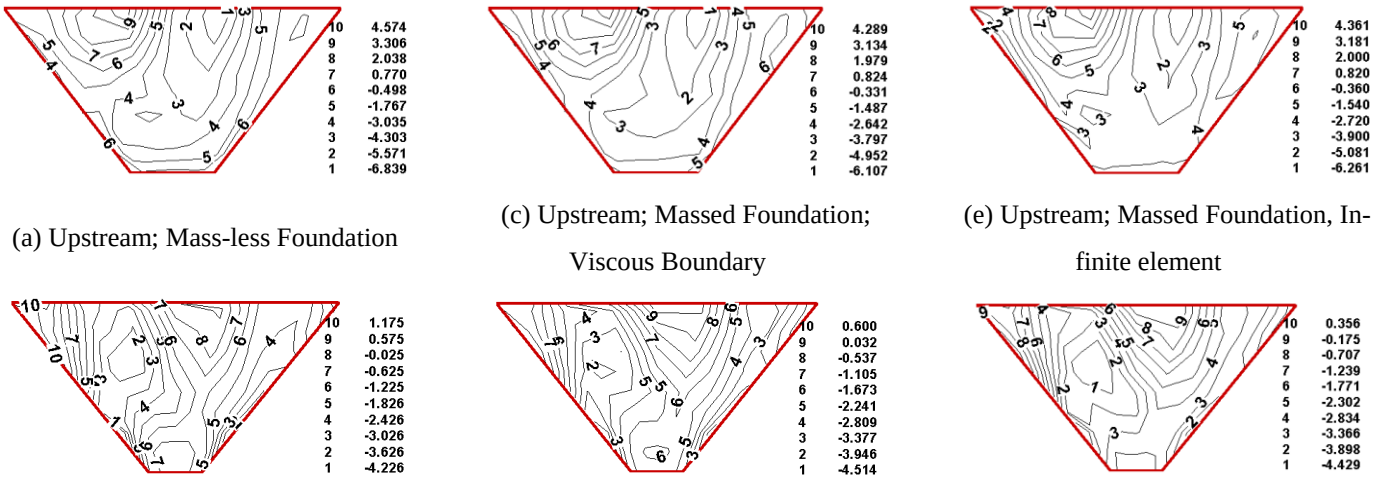

(a) Upstream; Mass-less Foundation

(c) Upstream; Massed Foundation; Viscous Boundary

(e) Upstream; Massed Foundation, Infinite element

(b) Downstream; Mass-less Foundation

(d) Downstream; Massed Foundation; Viscous Boundary

(f) Downstream; Massed Foundation, Infinite element

Figure 9. Foundation Mass effect on Seismic Arch Stress Contours (MPa)

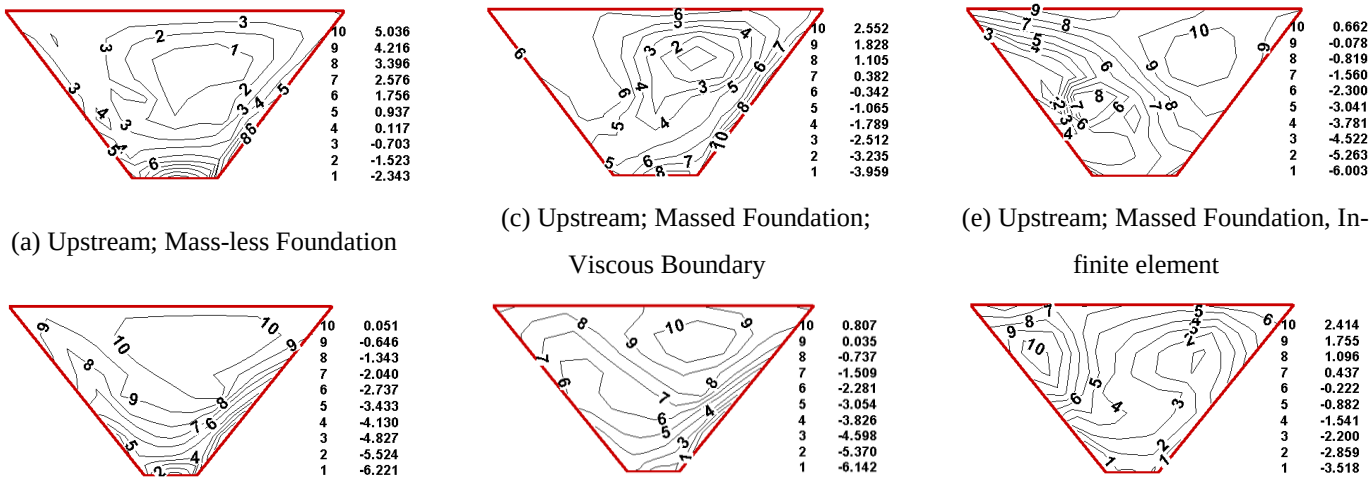

(a) Upstream; Mass-less Foundation

(c) Upstream; Massed Foundation; Viscous Boundary

(e) Upstream; Massed Foundation, Infinite element

(b) Downstream; Mass-less Foundation

(d) Downstream; Massed Foundation; Viscous Boundary

(f) Downstream; Massed Foundation, Infinite element

Figure 10: Effect of Foundation Mass on Seismic Cantilever Stress Contours (MPa)

Table 2. Maximum Tensile Dynamic Stresses

Stress direction	Foundation state	Value (MPa)
Arch	Mass-less Foundation	5.842
	Massed Foundation- Viscous Boundary	5.440
	Massed Foundation-Infinite Element	5.541
Cantilever	Mass-less Foundation	5.856
	Massed Foundation- Viscous Boundary	3.275
	Massed Foundation-Infinite Element	3.073

7 RESULTS OF NONLINEAR MODEL

Based on the results obtained from conducted nonlinear analyses, at the first load step, there is not any cracked Gaussian point due to the self-weight and the hydrostatic load. At the second load step, the system is excited simultaneously in the three directions using the components shown in Figure 7.

Figure 11 compares the time history of the crown crest displacement in the three directions. It can be observed that the model with massed foundation and infinite elements gives a lower response in comparison with the model assuming mass-less foundation.

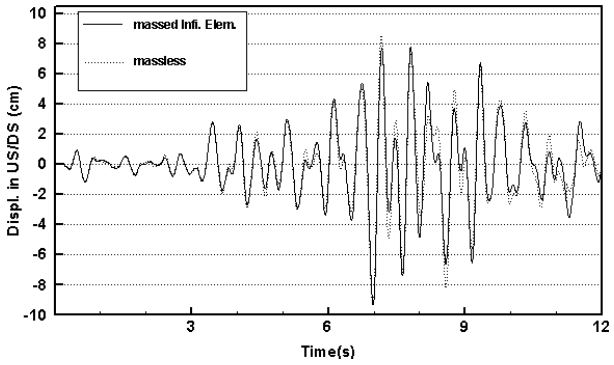

(a)

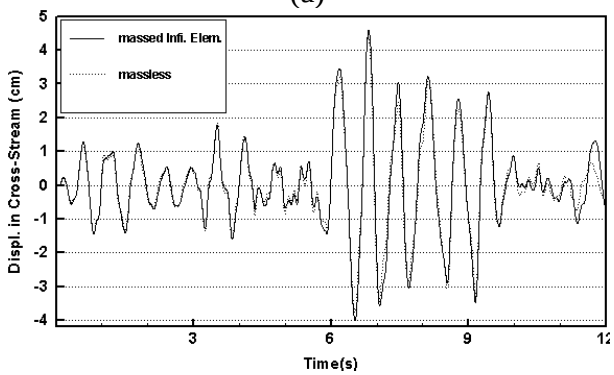

(b)

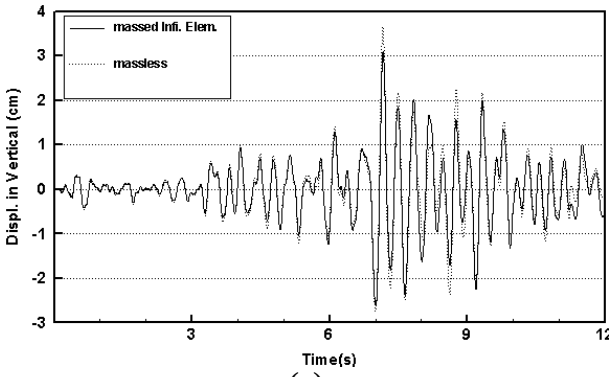

(c)

Figure 11: Crest Displacement of the Crown Cantilever; Nonlinear analysis, (a) US/DS component; (b) Cross-stream component; (c) Vertical component

It should be mentioned that the response of the two analyzed systems during the application of the self weight and the hydrostatic loads are linear and the Figure 11 does not include the static response of the two systems.

Figures 12 presents the crack profiles at the three layers of the Gaussian points through the thickness of the dam body when the foundation medium is assumed to be mass-less and Figure 13 shows the results when the massed foundation and infinite elements are used for modeling the near field of the semi-infinite medium.

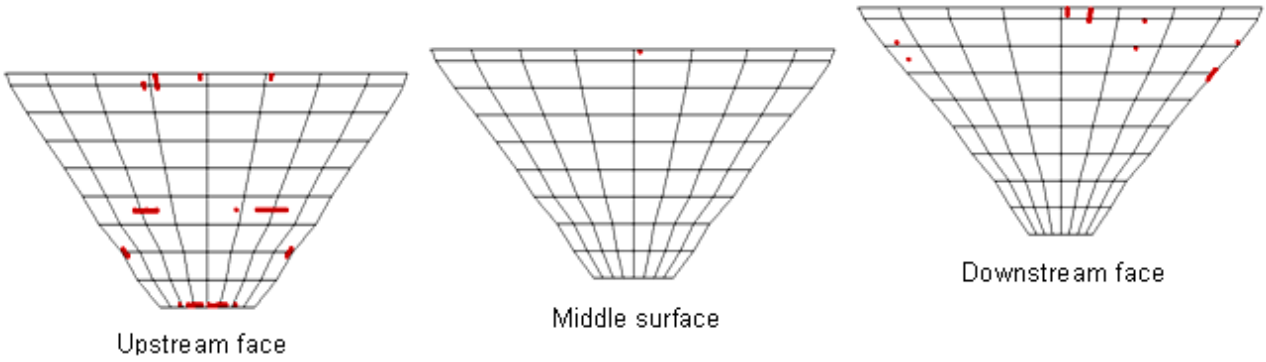

Figure 12: Cracked Profiles within the Dam Body; Mass-less Foundation

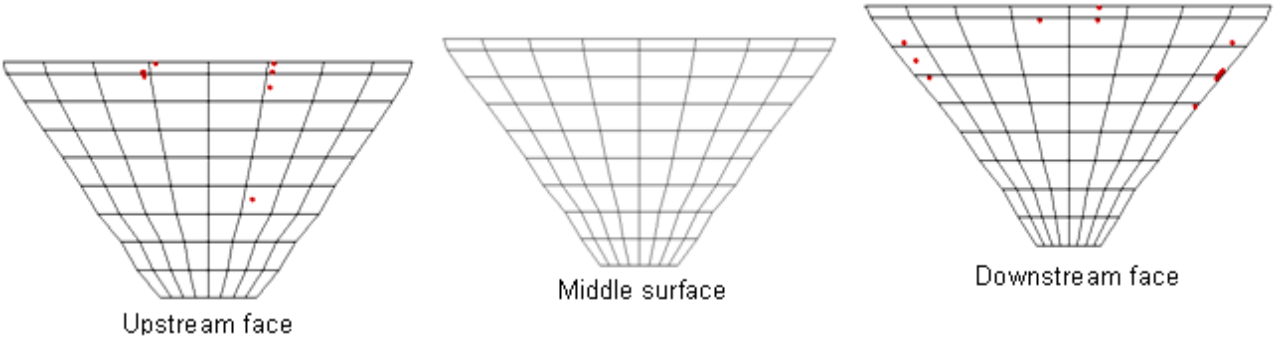

Figure 13: Cracked Profiles within the Dam Body; Massed Foundation Using Infinite Elements

Comparing the crack profiles shown in Figures 12 and 13, using massed foundation and infinite elements leads to less cracked Gaussian points which is a realistic conclusion. It is worth noting that in the model with mass-less foundation, the first crack occurred at 3.39s. However, the first crack in the second model (massed foundation including infinite elements) initiates at 6.855s. In fact, it makes sense because of larger response of the structure with mass-less foundation.

8 CONCLUSION

In the present paper, the FE model of the dam body, the reservoir and the foundation is excited using the three components of the earthquake recorded in Abbar station in Iran. The nonlinear behavior of the mass concrete is modeled using the smeared crack approach and the reservoir is assumed to be compressible. The three sets of models are analyzed to consider the effect of massed foundation on the seismic response of the system; the system with mass-less foundation, the system with massed foundation and applying viscous boundary on the far-end truncated boundary of the FE model of the foundation; and finally, the system with massed foundation utilizing infinite elements to simulate the effect of semi-infinite medium via the far-end truncated boundary of the foundation.

Based on the conducted analyses; modeling the foundation as a massed medium leads to less response with respect to the FE model with mass-less foundation. In linear analyses, cantilever stresses are reduced more than 40% when the foundation is assumed massed. However, this reduction in arch stresses within the dam body is less. In addition, the crack profiles within the dam body decreases intensely when the semi infinite medium via the far-end truncated boundary of the foundation is modeled using infinite elements.

It is worthy to note that one of the main problems in safety evaluation of concrete dams is larger estimation of the system response resulted from numerical methods than the real response of the system and the FE modeling of the foundation is one of the sources of these miss leading results. As shown, the proposed numerical algorithm is stable during the seismic analyses and can be utilized for seismic safety evaluation of concrete arch dams.

REFERENCES

Ardakanian R. , Ghaemian M. and Mirzabozorg H. “Nonlinear Behavior of Mass Concrete in 3D Problems Using Damage Mechanics Approach” European Earthquake Engineering, 2006, 2: pp. 89-65.

Antes, H. and Von Estorff, O., Analysis of Absorption Effects on the Dynamic Response of Dam Reservoir Systems by Boundary Element Methods , Earthquake Engineering and Structural Dynamics, Vol.15, pp. 1023-1036, 1987.

Bettess, P. “Infinite Elements” Penshaw Press, 1992, 1st ed.

Cervera M, Oliver J. and Faria R. “Seismic Evaluation of Concrete Dams via Continuum Damage Models” Earthquake Engineering and Structural Dynamics, 1995, 24: pp.1225–45.

Dungar R. “A Visco-Plastic Bounding Surface Model for Concrete under Compressive and Tensile Conditions and its Application to Arch Dam Analysis” Proceedings of Second International Conference on Constitutive Laws for Engineering Materials, Tucson/ AZ, 1987, pp. 849–856.

Espandar R. and Lotfi V. “Comparison of Non-Orthogonal Smeared Crack and Plasticity Models for Dynamic Analysis of Concrete Arch Dams” Computers and Structures, 2002, pp. 1461-1474.

Fok K.L., Hall J.F. and Chopra A.K., EACD-3D: A Computer Program for Three-Dimensional Analysis of Concrete Dams, Report No. UCB/EERC 86/09, University of California, Berkeley, 1986.

Fenves G. and Chopra A.K., Earthquake Analysis of Concrete Gravity Dams Including Reservoir Bottom Absorption and Dam-Water-Foundation Rock Interaction, Earthquake Engineering and Structural Dynamics, Vol. 12, No. 5, pp. 663-680, 1984.

Fenves G. and Chopra A.K., EAGD-84: A Computer Program for Earthquake Analysis of Concrete Gravity Dams, Report No. UCB/EERC 84-11, University of California, Berkeley, 1984.

Ghaemian, M., Noorzad, A. and Moghaddam, R.M. “Foundation Effect on Seismic Response of Concrete Arch Dams Including Dam-Reservoir Interaction” European Earthquake Engineering (EEE), 2006, 3: pp. 49-57.

Gaun, F., Moore, I.D. and Lin, G., Seismic Analysis of Reservoir-Dam-Soil Systems in the Time Domain, Coputer Metods and Advances in Geomechanics, Siriwardane & Zaman (eds), pp. 917-922, 1994.

Hall J.F. “Efficient Non-Linear Seismic Analysis of Arch Dams” Earthquake Engineering and Structural Dynamics, 1998, 27: pp.1425–1444.

Kuo JSH. “On the Nonlinear Dynamic Response of Arch Dams to Earthquakes–I. Fluid–Structure Interaction: Added-Mass Computations for Incompressible Fluid. II. Joint Opening Nonlinear Mechanism: Interface Smeared Crack Model” Ph.D. Thesis, University of California, Berkeley, 1982.

Mirzabozorg, H., Khaloo, A.R., Ghaemian, M. and Jalalzadeh, B. “Non-Uniform Cracking in Smeared Crack Approach for Seismic Analysis of Concrete Dams in 3D Space“ European Earthquake Engineering, Accepted to be published, 2007.

Mirzabozorg H. and Ghaemian M. “Nonlinear Behavior of Mass Concrete in Three-Dimensional Problems Using Smeared Crack Approach” Earthquake Engineering and Structural Dynamics, 2005, 34: pp. 247-269.

Mirzabozorg H., Ghaemian M. and Kianoush, M.R. “Damage Mechanics Approach in Seismic Analysis of Concrete Gravity Dams Including Dam-Reservoir Interaction” European Earthquake Engineering, 2004, XVIII (3): pp. 17-24.

Mirzabozorg H., Khaloo A.R. and Ghaemian M. "Staggered Solution Scheme for Three-Dimensional Analysis of Dam-Reservoir Interaction" Dam Engineering Journal, 2003, XIV (3): pp. 1-33.

Mirzabozorg, H., Ghannad M.A. and Ghaemian, M., Foundation Interaction Effect on the Seismic response of Amir-Kabir Arch Dam, Proceedings of the Fourth International Conference on Earthquake Engineering and Seismology, Tehran, Iran, May 12-14, 2003.

Noruziaan B. "Nonlinear Seismic Analysis of Concrete Arch Dams" Ph.D. Thesis, Department of Civil and Environmental Engineering, Carleton University, Ottawa, Canada, 1995.

Tan, H. and Chopra, A.K. "Earthquake Analysis of Arch Dams Including Dam-Reservoir-Foundation Rock Interaction" Earthquake Engineering and Structural Dynamics, 1995, 24: pp. 1453-1474.

Tan, H. and Chopra, A.K. "Dam-Foundation Rock Interaction Effects in Frequency-Response Functions of Arch Dams" Earthquake Engineering and Structural Dynamics, 1995, 24: pp. 1475-1489.

Ross M., Modeling Methods for Silent Boundaries in Infinite Media, ASEN 5519-006: Fluid structure interaction, 2004.